ACES Asian Chemical Editorial Society

doi.org/10.1002/cnma.202200532

CHEMNANOMAT
Research Article

www.chemnanomat.org

NIR-triggered Synergetic Photothermal and Chemotherapy Cancer Treatment Based on SiO_2@Au@SiO_2@QDs-DOX Composite Structural Particles

Xinbing Jiang,[a] Lu Qiao,[b] Huan Yang,[c] Ben Q Li,*[d] and Shujiang Ding*[a]

Abstract: This paper reports the synthesis of multi-layer SiO_2@Au@SiO_2@QDs nanoparticles with a dual-functionality of simultaneous heating and temperature sensing and their applications to in vitro chemo-thermal therapy. The heating is activated by a NIR-light through resonance excitation of surface plasma while in-situ thermal sensing is accomplished by the QDs photoluminescent (PL) effect. These dual function nanoparticles are used as a drug carrier for in vitro chemo-therapy-photothermal co-treatment for malignant cells. A comparative study of drug release profiles was performed with and without 808 nm laser irradiation. The drug release rate was accelerated by a rise of temperature, which is induced by plasmonic heat generation associated with Au nanoshells; while the temperature change is monitored by the QD nanoparticles at the same time. The results showed that SiO_2@Au@SiO_2@QDs-DOX platform enabled the combination of local specific chemotherapy with external near-infrared (NIR) photothermal therapy and significantly improved the efficacy of cancer treatment. This combined treatment demonstrated synergistic chemotherapeutic-thermal effects compared to chemotherapy or photothermal therapy alone, resulting in higher efficacy.

Introduction

Chemotherapy is a major treatment for cancer cells. However, nonspecific chemotherapy can have many undesired side effects on normal tissues and cells, such as hair loss, nausea, vomiting, and heart damage.[1] To overcome this limitation, combination therapies with targeted and/or controlled delivery of agents have been developed. One of the effective combination therapies is thermotherapy using photothermal agents, which is well suited to suppress tumor cells in specific localized areas, thus minimizing damage to adjacent normal tissues and cells.[2]

It is known that the NIR-absorbing photothermal agents, such as carbon- or gold-based nanomaterials, may be used as heat carriers for hyperthermia.[3] Upon irradiation by an NIR laser, these materials can convert light into heat that ablates cells, which in turn inhibits the growth of cancer cells.[4] Enyi Ye had synthesized plasmonic gold nanocrosses with strong near-infrared absorption, targeted the gold nanocrosses onto multi-drug-resistant bacteria and their biofilms, and achieved effective ablation of drug-resistant bacteria and their biofilms by using their photothermal effects.[5] However, these reported photothermal agents can provide heat to the tumorigenic zone, but lack a real-time temperature rise detection feedback system. This uncontrolled heat therapy can also lead to undesired non-specific damage and ablation of surrounding normal tissue. Therapeutic approaches that deliver chemotherapeutic agents and controlled thermal doses to the cancer area are expected to improve efficacy; the extent of the improvement would depend how the chemo-thermal therapy can be synergistically delivered. To achieve a desired therapy effect with no or minimum side effect, systems capable of co-delivery of chemotherapy agent with quantitative thermal delivery of photothermal therapeutic agent are needed and have been in literature.[6] Chung et al. have fabricated protein-functionalized modified reduced graphene oxide nanosheets,[7] and Qian et al. have developed gold nanorods and doxorubicin co-loaded polymersomes to combine photothermal therapy and chemotherapy in a good way.[4a] To achieve the combination of chemotherapy and thermotherapy, the design of drug loading structures and controlled release system for chemotherapeutic agents becomes critical. The relevant prospective work is reviewed by Zibiao Li.[8] Although the synergistic therapeutic effects of these composite nanostructures have been demonstrated in many in vitro and in vivo studies, the nanomaterials reported in these studies lack real-time thermal monitoring. Real-time measurement and control of heat during chemotherapeutic-thermal treatment would further improve the delivery of quantitative thermal doses and the release of chemotherapeutic agents, thereby increasing the efficiency of the combination therapy.

Freddi has developed single-particle nanothermometers, which are envisioned as organic fluorescent dyes embedded in the shell of polymer-coated nanoheaters.[9] In his approach, gold nanorods and gold nanostars were used as nanoheater

[a] Dr. X. Jiang, Prof. S. Ding
School of Chemistry, Xi'an Key Laboratory of Sustainable Energy Materials Chemistry Xi'an, Xi'an Jiaotong University, Xi'an 710049, Shaanxi Province (P. R. China)
E-mail: dingsj@mail.xjtu.edu.cn

[b] Dr. L. Qiao
Department of Gastroenterology, Second Affiliated Hospital of Xi'an Jiaotong University, Xi'an, 710004, Shaanxi Province (P. R. China)

[c] Dr. H. Yang
School of Physics and Optoelectronic Engineering, Xidian University, Xi'an 710071, Shaanxi Province (P. R. China)

[d] Prof. B. Q Li
Department of Mechanical Engineering, University of Michigan, Dearborn, MI 48128 (USA)
E-mail: benqli@umich.edu

and rhodamine B was adsorbed onto the surface of negatively charged polymer shells and used as a thermometer. Nigoghossian et al. devised a similar structure for surface-attached thermometers, except that in his approach its heating element is in the shell of the nanoparticle and the temperature measurement probe is the core nanoparticle rather than the molecular dye.[10] The heated part is gold-coated silica nanoparticles with a size of 283 nm (gold nanoshells), and the temperature-sensitive part is $NaGdF_4:Yb^{3+}:Er^{3+}$ upconversion nanoparticles coated with a 7 nm silica layer. Rosal et al. abandoned the use of surface attachment and instead used a polymer shell to encapsulate the heater nanoparticles and the thermometric nanoparticles.[11] In his design scheme, the temperature sensing probes are Nd^{3+}-doped $NaGdF_4$ nanoparticles, PbS/CdS/ZnS QDs are used as heaters, and the polymer matrix is poly(lactic acid-glycolic acid) (PLGA).

Using QDs' thermal sensitive properties to monitor the delivery of thermal dose during tumor cell thermotherapy is possible and has been demonstrated in several prospective studies. Daniel Jaque had used CdSe QDs fluorescence thermometry for real-time intracellular temperature read-out during gold nanorod plasma-mediated photothermal therapy for tumor cells. This precise temperature read-out provides the possibility of settling operation limits for laser-induced hyperthermia processes, avoiding the creation of irreversible thermal damage in surrounding healthy cells and tissues.[12] A yet unexplored capability of near-infrared emitting semiconductor nanocrystals (quantum dots, QDs) is demonstrated by Blanca del Rosal.[13] Temperature self-monitored QD-based photothermal therapy (PTT) is presented for the first time using PbS/CdS/ZnS QDs emitting in the second biological window. These QDs are capable of acting, simultaneously, as photothermal agents (heaters) and high-resolution fluorescent thermal sensors, making it possible to achieve full control over the intratumoral temperature increment during PTT. In our previously published study, a certain concentration of SiO_2@Au@SiO_2@QDs composite particles were ingested into cells, and then the intensity of laser was adjusted to achieve different thermal doses delivered. During this process, real-time cell temperature changes were obtained by monitoring the temperature-sensitive fluorescence of the composite particles, so that the fluorescence changes of the composite particles could actually be monitored to control the delivered thermal dose in the cells.[14] Therefore, it is feasible and practical to wrap temperature-sensitive QDs on the surface of composite particles to monitor temperature changes in vivo and in vitro in real time.

Although the heating and temperature sensing functions are conducted simultaneously by two different components in a single nanoplatform in the corresponding system described above, these composites do not have drug loading capacity, specifically, chemotherapeutic agents may not be loaded onto these nanoparticles to achieve the effect of synergistic treatment of chemo-photothermal combine therapy.

In this work, we constructed the SiO_2@Au@SiO_2@QDs-DOX composite platform as a synergistic therapeutic tool to deliver drugs and quantitative heat to the tumorigenic zone, which in turn activates combined chemo-photothermal treatment of tumor cells. In the construction of SiO_2@Au@SiO_2@QDs-DOX, the component core SiO_2@Au gold nanoshells were used as nanoheater and the attached CdTe/CdS/ZnS QDs function as nanothermometers. The chemotherapeutic agent DOX is loaded onto the composite dual-functional nanoparticle SiO_2@Au@SiO_2@QDs to render the final nanostructure with capability of synergistic chemo-thermal therapy with real time thermal sensing. Cancerous cells incubated with DOX-loaded SiO_2@Au@SiO_2@QDs were irradiated with near-infrared (NIR) illumination on with these combined agents and temperature is measured by QD thermometers. Results show that significantly greater cancerous cell destruction was observed than either chemotherapy or photothermal treatment only, which is attributed to both SiO_2@Au@SiO_2@QDs-composite particle-mediated photothermal ablation and photoexcitable thermally triggered DOX release.

Results and discussion

Synthesis and characterization of SiO_2@Au@SiO_2@QDs dual-functional particles

The multi-layer structure of this composite particle is illustrated in Scheme 1. The whole synthesis process involves three parts which contains the plasmonic heating gold shell preparation, the silica spacing layer coating and the thermometric QDs anchoring. For the gold shell preparation, the "seed and growth" method was employed which was first presented by Halas.[15] Three steps are involved, including APTMS modification, seeds anchoring and shell growth. Among these steps, the APTMS functionalization is a critically important step that affects the following anchoring seeds, which in turn affects the Au-shell growth.[16] In our previous study, a non-uniform surface modification by APTMS would result in uneven seed sites, leading to the formation of an undesired half-baked shell.[17] A complete gold nanoshell, prepared as described above with proper APTMS surface functionalization, was visualized by TEM as shown in Figure 1(a). A rather spherical solid gold shell with a size of 220 nm was obtained. FRET (fluorescence resonance energy transfer) effect would appear when QDs were directly attached on the solid gold nanoshells, resulting in QDs' emission photobleaching. This is because the characteristic absorption spectrum of the gold nanoshell acceptor overlaps with the fluorescence peak emission spectrum of the QDs donor, the gold nanoshell will absorb the emission energy of the QDs, resulting in QDs' fluorescence quenching.[18] According to the literature, and also confirmed by our experiments, QDs need to be placed at least 10 nm away from the gold surface if the donor-acceptor FRET effect is to be eliminated.[14] Although many options are available, the silica layer was selected as the separator for gold/QDs in this study mainly because of its known good biocompatibility. For silica coating, a polymer-mediated approach, in which involves the use of amphipathic non-ionic surfactant PVP, was conducted to pretreat the as-prepared gold shell. Then these PVP-treated gold shells were transferred to the classical Stöber reactive phase for silica layer

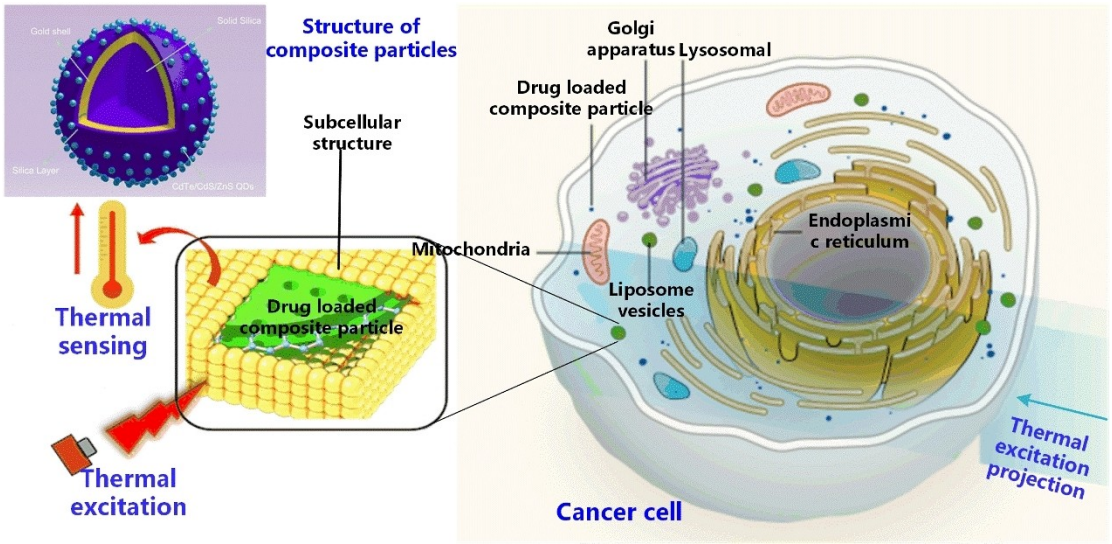

Scheme 1. Structural sketch of SiO_2@Au@SiO_2@QDs-DOX composite particle and the application for photothermal-chemotherapy synergistic treatment.

growth. The thickness of the coated silica layer can be adjusted by the additional frequency of silicon source. TEM image of as-prepared SiO_2@Au@SiO_2 particle was shown in Figure 1(b) with a thickness of 15 nm silica coating.

For the anchoring of thermosensitive CdTe/CdS/ZnS QDs (hereafter referred to as QDs unless otherwise stated), a PAH-mediated layer-by-layer self-assembly method was used to achieve the immobilization of QDs on the SiO_2@Au@SiO_2 surface by electrostatic interaction. From Figure 1(c), it can be clearly seen that a thicker particle surface is obtained after electrostatic adsorption of QDs compared to SiO_2@Au@SiO_2 particles. The lattice of adsorbed QDs can be seen in the TEM image at magnification, which is also good evidence that the QDs have been successfully immobilized on the surface of the silica layer (see inset of Figure 1(c)). In SI, scanning electron microscopy of above three kinds of particles were provided and statistical calculations of their particle size distribution were performed by ImageJ software.

To further verify the successful coating of silica and the successful anchoring of QDs, energy dispersive X-ray spectroscopy (EDS) characterization was performed, and the results obtained are shown in Figure 1. Figure 1(d) shows the TEM image of a single SiO_2@Au@SiO_2@QDs composite particle, and Figure 1(e–l) gives the distribution of the constituent elements of the particle. A closer look at Figure 1 (f, g and h) shows that the distribution area of Si and O elements is larger than the mapped area of Au and overlaps with the Au area, which also indicates that the silica layer is encapsulated on the gold shell surface. As seen in Figure 1(e) and (j-l), the largest distribution area of the constituent elements of the adsorbed quantum dots and their uniform distribution in the outermost layer of the particles indicate that the QDs are successfully attached to the surface of the silica coating. Energy dispersive spectrometer (EDS) plots show the coexistence of the constituent elements, which proves the successful preparation of SiO_2@Au@SiO_2@QDs. The mass ratios and atomic ratios of the constituent elements are quantified in Figure 1(m), and the results further confirm the success of the silica layer cladding and subsequent anchoring of the QDs. From Figure 1(m), it was found that the elements of Zn, Cd, S and Te were uniformly distributed in the circular area, which suggested the CdTe/CdS/ZnS QD was evenly anchored onto the swept core-shell particle. However, the atomic percentage ratio of Zn:Cd:S:Te = 0.93:1.68:1.66:0.18, seems not consistent with the molar ratio of CdTe/CdS/ZnS QDs. It can be understood in the following two aspects. Firstly, reviewing the entire QD's synthesis pathway, the synthesis of CdTe/CdS/ZnS QDs was started from CdTe core, followed by the addition of the CdS and ZnS precursor for the formation of CdS and ZnS shells step by step. During the synthesis reaction process, mercaptosuccinic acid (MSA) and mercaptopropionic acid (MSA) are involved as surface stabilizers, and the presence of S in mercapto group inevitably pulled up the overall S-atom ratio.[19] Additionally, as Yalcin's study showed that the diffusion of Zn into the inner layer occurred simultaneously with the evaporation of Cd and S during the synthesis of CdSe-CdS-ZnS core-multilayer shell QDs, which in turn led to the $Cd_xZn_{1-x}Se$-$Cd_yZn_{1-y}S$ core-shell QDs. Here, based on the similarity of the synthesis methods, it is possible and trustworthy that the diffusion of Zn into the inner layer along with the evaporation of Cd and S also occurs during the synthesis of CdTe–CdS–ZnS core-multilayer-shell QDs. The prepared QDs are possibly with more complex crystalline structure like $Cd_xZn_{1-x}Te/Cd_yZn_{1-y}S$, rather than the standard structure of CdTe/CdS/ZnS.[20]

Starting from SiO_2@Au, the absorption and PL spectra of different particle solutions were measured and plotted in Figure 2. Here it can be seen that the absorption spectrum of the SiO_2@Au@SiO_2@QDs composite particle also has a broad absorption band from 700 nm to 1100 nm, which is similar to that of SiO_2@Au and SiO_2@Au@SiO_2 particles, which would

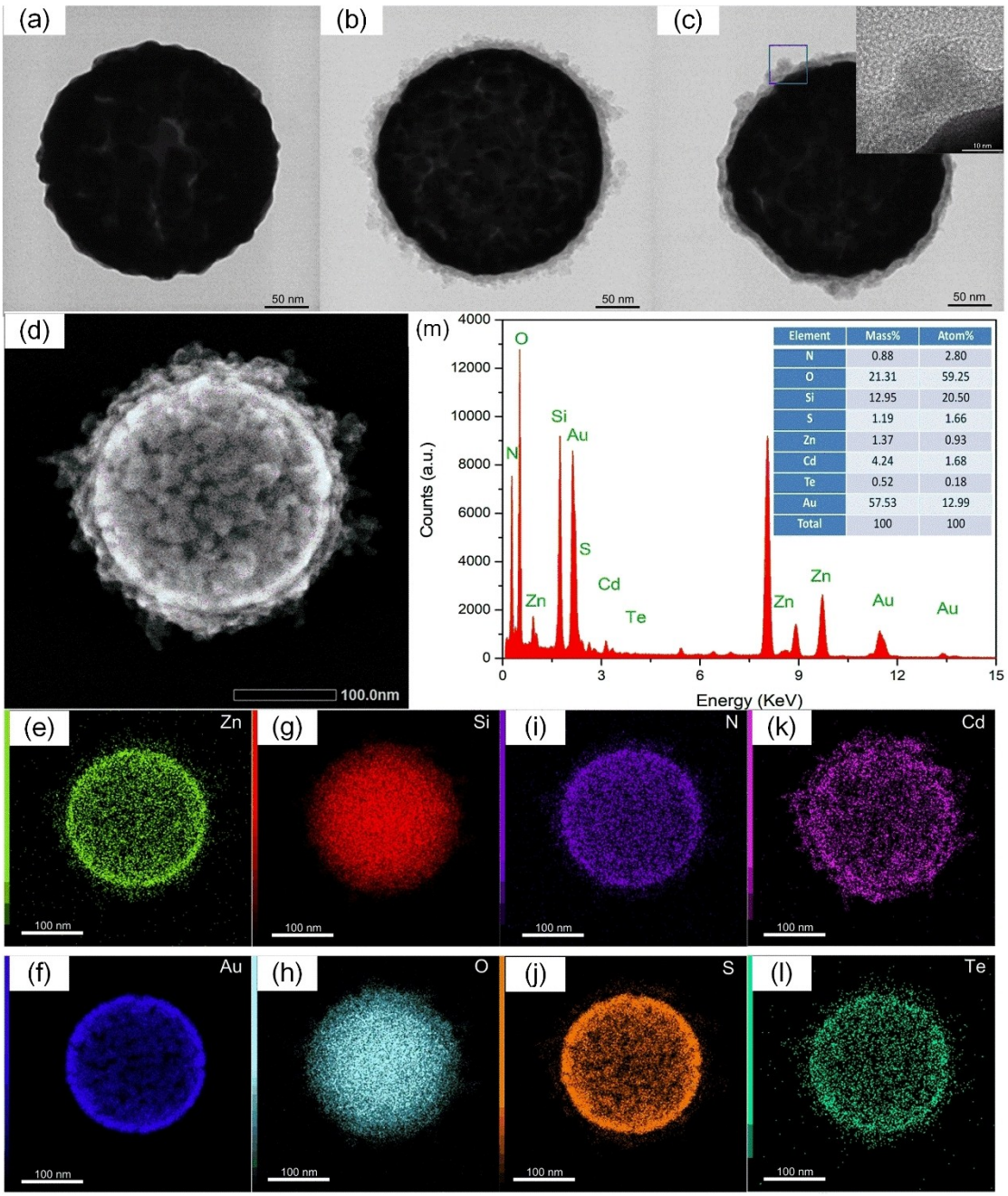

Figure 1. Transmission electron microscopy morphology and mapping characterization. TEM images of (a) SiO_2@Au, (b) SiO_2@Au@SiO_2 and (c) SiO_2@Au@SiO_2@QDs, the inset shows the enlarged TEM image in the blue box in (c). (d) TEM image of SiO_2@Au@SiO_2@QDs particle, (e-l) EDS mapping images of SiO_2@Au@SiO_2@QDs composite particles composed of elements Zn, Au, Si, O, N, S, Cd and Te. (m) Mass ratios and atomic ratios of the complete elemental distribution.

suggest that it can also be used as a plasmonic heater for photothermal therapy (see Figure 2(a)). From the Figure 2(b), The PL peak wavelength of the freely dispersed QDs is located at 585.0 nm, while the PL peak wavelength position of the composite particles undergoing the anchoring process is red-shifted to a lower energy position of 589.8 nm. This peak position difference may be attributed to the existence of aggregate structure result from the change of the surrounding environment.[21] The presence of the silicon dioxide coating increases the spacing between the gold shell and the attached QD, which also weakens the PL plunge caused by FRET.[22] As can be seen from the figure, only a 21% decrease in the fluorescence intensity of the composite particle solution with a 15 nm thickness of silica shell layer occurred compared to the pure QDs solution. For the quantification of the content of QDs on the complex, it is sufficient to calibrate and measure the concentration of quantum dots before and after adsorption. A previous prospective study presented by Xiaogang Peng can be

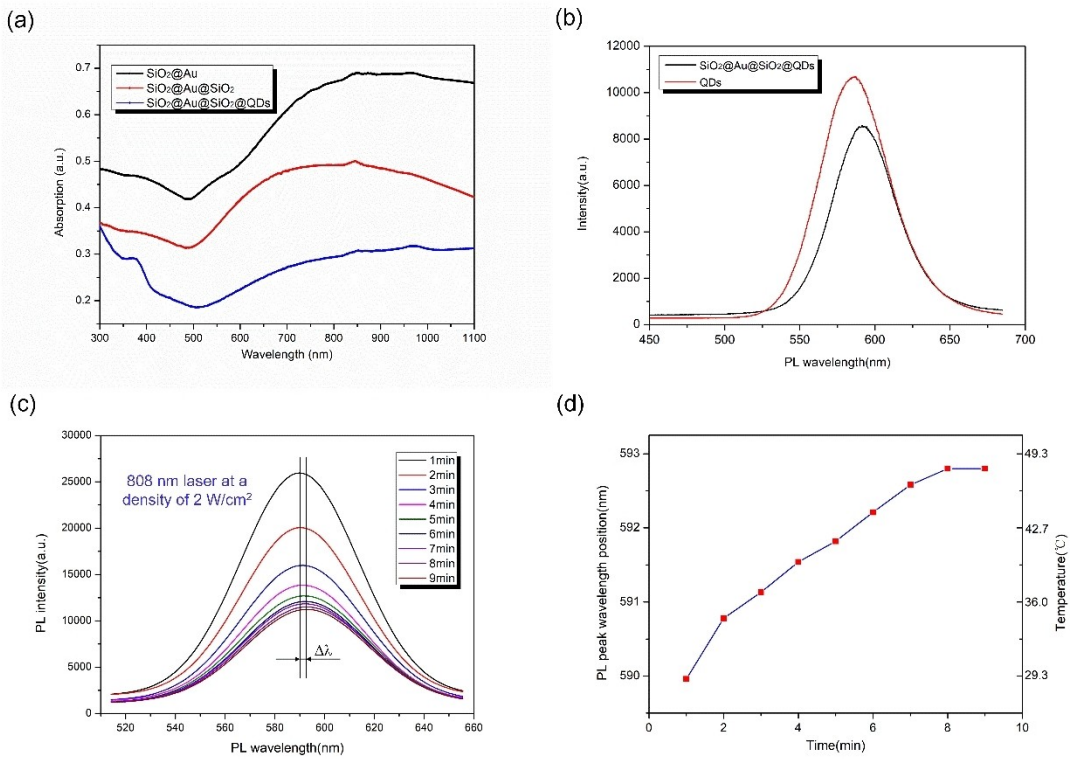

Figure 2. Optical properties characterization of the prepared particles. (a) UV-Vis absorption spectra of SiO_2@Au, SiO_2@Au@SiO_2 and SiO_2@Au@SiO_2@QDs particles. (b) PL spectra of SiO_2@Au@SiO_2@QDs and the attached CdTe/CdS/ZnS QDs. (c) The PL evolution and (d) temperature evolution of SiO_2@Au@SiO_2@QDs response to the irradiation of 808 nm laser at a density of 2 W/cm^2.

referred which is based on the extinction coefficient of quantum dots and Lambert's law to achieve the experimental determination of the concentration of QDs.[23] The amount of quantum dots adsorbed on the complex is obtained by subtracting the concentration of quantum dots in the supernatant after adsorption from the concentration of unabsorbed QDs. The concentration of adsorbed QDs can be calculated as 0.462 μM. The specific quantification process can be found in SI.

Thermometry calibration of the SiO_2@Au@SiO_2@QDs composite particles

Before using SiO_2@Au@SiO_2@QDs composite particles for quantitative measurements of temperature in the area to be measured, the thermal PL sensitivity of the composite particles needs to be calibrated. The detailed procedure of the sensitivity calibration was reported in a previous paper.[24] The relationship between the temperature and the PL peak wavelength position was shown in the following equation:

$$W_{PL} = 585.6 + 0.15T \quad (1)$$

where W_{PL} is the PL peak wavelength and T is the local temperature in °C. The slope of the fitted straight line of 0.15 nm/°C represents the thermally induced spectral shift coefficient of the composite particle.

After calibrating the thermal sensitivity of this composite particle, the photothermal heating and simultaneous PL thermometry experiment was conducted. The collected PL evolution of SiO_2@Au@SiO_2@QDs response to the irradiation was shown in Figure 2, which the PL peak wavelength positions had a significant red shift with increasing irradiation time. For clearly show the relationship between the PL peak wavelength and irradiation time, the peak positions were extracted from Figure 2(c) and plotted in Figure 2(d). The corresponding temperature reading according to the calibration relational expression (1) was list on the right side of Y-axis, from which the temperature had an evident raise along with the PL peak position redshift during the exposure process. For the initial stage, the PL peak position was located at 589.6 nm which indicated at a start temperature at 26.7 °C. After about 8 min exposure, the peak position was shifted to 592.8 nm and stayed unchanged which means a thermal equilibrium had been reached and the steady state temperature was kept at 48.0 °C. Through this confirmatory experiment, the fact that this composite particle possessed dual-functional properties was further verified and can be laid the foundation for the next application experiment.

Light-triggered drug release study of drug-carrying particles

To study the drug release behavior of composite particles, doxorubicin (DOX), an anticancer drug, was chosen as a model drug loaded on the surface of SiO_2@Au@SiO_2@QDs (i.e. SiO_2@Au@SiO_2@QDs-DOX). The drug-carrying capacity was determined by measuring the UV-vis absorption spectrum of DOX at 480 nm.[25] And it can be evaluated by following formula:

$$\text{Loading \%} = \frac{\text{Total amount of DOX added} - \text{Amount of DOX in redispersed pellet}}{\text{Total amount of DOX added}} \times 100\%$$

Figure 3(a) shows the UV-vis absorption spectra curves of SiO_2@Au@SiO_2@QDs-DOX, SiO_2@Au@SiO_2@QDs and DOX dispersions, from which the absorption value was extracted and the loading efficiency (that is, the ratio of the absorption values) was also calculated. The loading level of the drug was also investigated by the characteristic DOX optical absorbance at ~480 nm. The absorbance value of DOX aqueous solution with a concentration of 1 mg/mL at 480 nm is 3.53, while the absorbance value of the SiO_2@Au@SiO_2@QDs and SiO_2@Au@SiO_2@QDs-DOX compound nanoparticles at 480 nm before and after drug loading are 0.01 and 0.255. Assuming that the pure 1 mg/mL DOX aqueous solution is 100% drug loaded, the drug loading efficiency of the compound nanoparticles can be calculated as

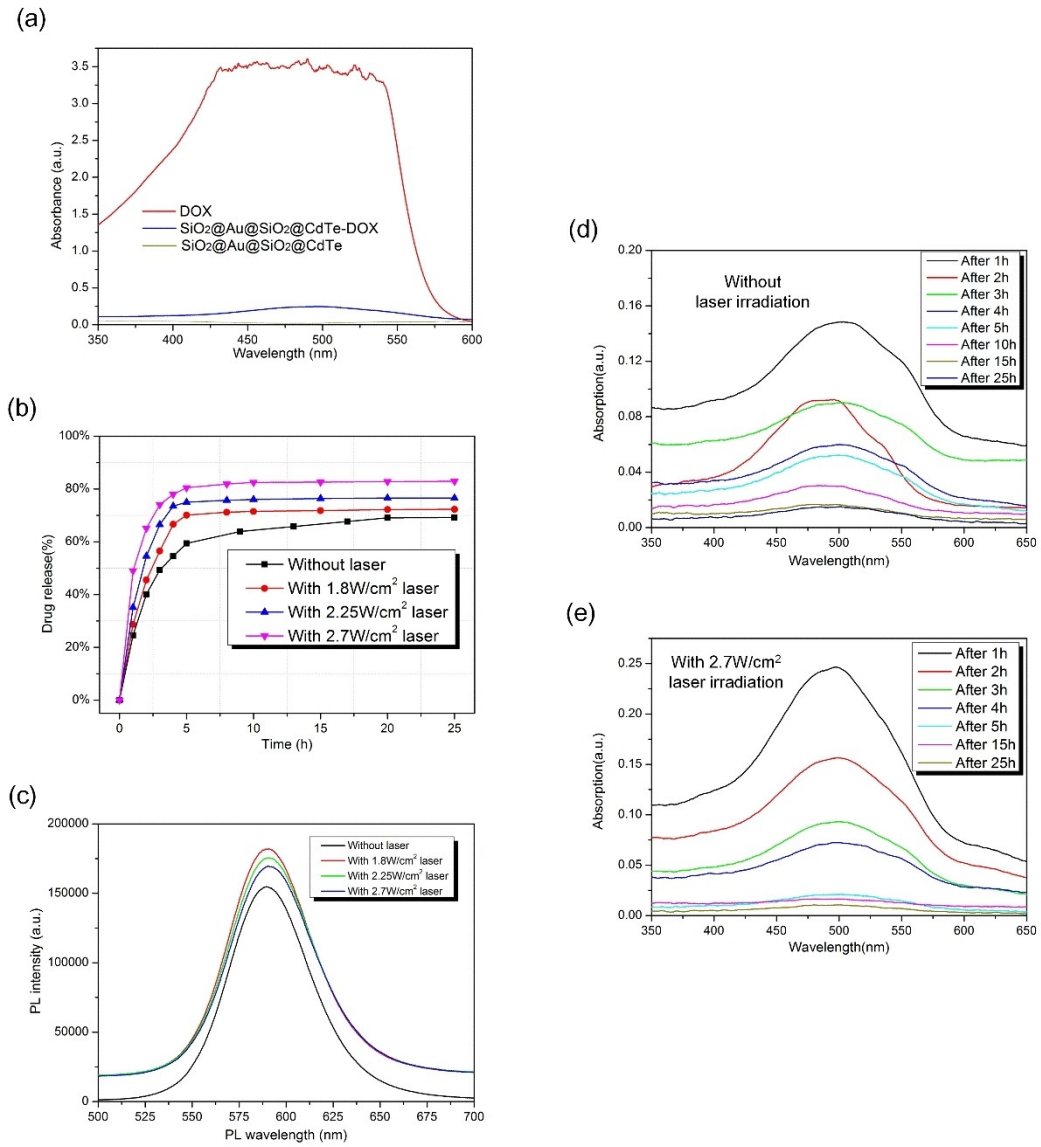

Figure 3. (a) UV-Vis absorption spectra of SiO_2@Au@SiO_2@QDs-DOX and DOX aqueous solution. (b) Time-histories of DOX drug release from SiO_2@Au@SiO_2@QDs-DOX with and without 808 nm laser irradiation at different time intervals. (c) PL spectrum curves of SiO_2@Au@SiO_2@QDs-DOX under laser irradiation with different power density. UV-Vis absorption spectra evolution of the supernatant solution (d) without and (e) with 2.7 W/cm^2 laser irradiation. The concentration of the SiO_2@Au@SiO_2@QDs used for drug loading is 0.3 mM.

$$Loading\ efficiency = \frac{0.255 - 0.01}{3.53} = 7.2\%$$

After knowing the drug loading efficiency, the loading drug dose can be calculated by the following equation.

$$Loading\ drug\ dose = Loading\ efficiency \times 1mg/mL$$
$$= 0.072\ mg/mL$$

According to the above calculation of the drug load, DOX in the supernatant drug release process can be estimated by the following equation:

$$Drug\ dose\ in\ supernatant = \frac{The\ absorbance\ of\ supernatant\ at\ 480\ nm}{3.53} \times 1mg/mL$$

Since the drug loading of the composite particles has been calculated, the amount of DOX drug in the supernatant can also be calculated according to the following equation:

$$Drug\ dose\ in\ supernatant$$
$$= Drug\ release\ efficiency \times 0.072mg/mL$$
$$= Drug\ release\ efficiency \times 72\mu g/mL$$

To understand the thermal effect on the DOX drug release, the composite particles loaded with DOX were excited by a NIR laser of 808 nm, which raised the temperature of the composite colloids through resonance plasmonic heating. The drug release histories with and without laser irradiation (or plasmonic heating) were recorded as shown in Figure 3(b). Inspection of the figure clearly indicates that the drug release rate experiences a significant increase with laser-induced resonance heating than without. When unheated, the DOX has a natural release of ~69.2% (49.824 μg/mL). As a comparison, laser induced heating with a power density of 1.8, 2.25 and 2.7 W/cm^2, gives rise to a corresponding release of 72.3% (52.056 μg/mL), 76.6% (55.152 μg/mL) and 82.9% (59.688 μg/mL), respectively. PL spectrum curves of SiO_2@Au@SiO_2@QDs-DOX solution under different power density laser irradiation were collected and illustrated in Figure 3(c). By examining Figure 3(c), a power density of 1.8 W/cm^2 produces plasma thermally induced PL peak wavelength position shift to 590.8 nm, 2.25 W/cm^2 for 591.6 nm and 2.7 W/cm^2 for 592.3 nm. Based on the relationship between PL peak wavelength and temperature obtained by the previous calibration process (the equation (1)), PL peak wavelength positions of 590.8 nm, 591.6 nm and 592.3 nm indicated temperature rise to 34.7 °C, 40 °C and 44.7 °C, respectively. From the above results, it can be concluded that a greater laser density leaded to a lower energy level of PL peak wavelength position, indicating reached a higher temperature. And then a higher temperature further provides more energy to break the binding between DOX and the drug-loaded particles and accelerates more drug release from the particles, yielding higher release rates.

To further evaluate the effect of plasmonic heating on the DOX release, the absorption spectra of supernatant with and without 2.7 W/cm^2 laser irradiation were collected and included in Figure 3(d) and (e). From Figure 3(e), under irradiation of a power density of 2.7 W/cm^2, the absorption of the supernatant solution decreases down to zero in a time interval of 5 h, indicating it takes only 5 h to complete the drug release. Comparatively, it took about 15 h to reach zero (see Figure 3(d)) for the case of without laser irradiation. Cross-examination of Figures 3(b and e) shows that it took about 5 h to achieve the release of drug dose (i.e. ~82.9%) under 2.7 W/cm^2 laser irradiation. However, for the case of without irradiation, the release ratio reduced to ~69.2% and the release time increased to 15 h. This confirms that the temperature increase induced by plasmonic photothermal heating leads to more drug release with an accelerated speed, which means large concentrations of drugs can accumulate in the diseased tissue in a short period of time that is beneficial for cancer chemotherapy treatment.

For intracellular thermometry in optical hyperthermia, the concentration-dependent cellular uptake of SiO_2@Au@SiO_2@QDs was investigated and shown in Figures 4(a-c). From Figures 4(a–c), this is evident through confocal microscopy images: cellular uptake is significantly influenced by the concentration of composite particles, indicating that HOS cells treated by 0.6 mM composite particles showed the highest uptake efficiency. Though a higher concentration of particle can acquire a more loading capacity, the more loading would affect the cellular state. Hence, an appropriate concentration of particle should be selected to balance the loading capacity and the consequent cellular effect. For investigating the relationship between the uptake efficiency and the incubation time, HOS cells were treated with 0.4 mM SiO_2@Au@SiO_2@QDs and incubate for different time, and then were fixed and sliced, finally visualized by TEM characterization (see in Figures 4(d–f)). Inspection of the TEM images showed in Figure 4(d–f), the cellular uptake efficiency had an evident incubation time dependent property. The number of ingested particles showed a clear time-dependent characteristic, with a gradual increase in the number of ingested particles with increasing incubation time. For getting a more ingestion ration, extension of the incubation time should be considered.

In vitro chemo-photothermal therapy

For cell viability measurement, HOS cells were injected into 96-well plates at a density of 1×10^4 cells/well and allowed to grow overnight at 37 °C and 5% CO_2. Subsequently, the composite particles dispersed in the culture medium were added to the cell culture dishes and incubated for 4 hours. An 808 nm laser was used as the excitation light source to irradiate the cells at a density of 1.5 W/cm^2 for 5 min. After irradiation, the plates were returned to the incubator and incubated for another 24 h. CCK-8 assay was selected for evaluating the in vitro anti-tumour efficiency. Blank particles, i.e. particles not loaded with drug (simply labelled as SiO_2@Au@SiO_2@QDs) showed no cytotoxicity to HOS cells at the stated concentrations, which would also

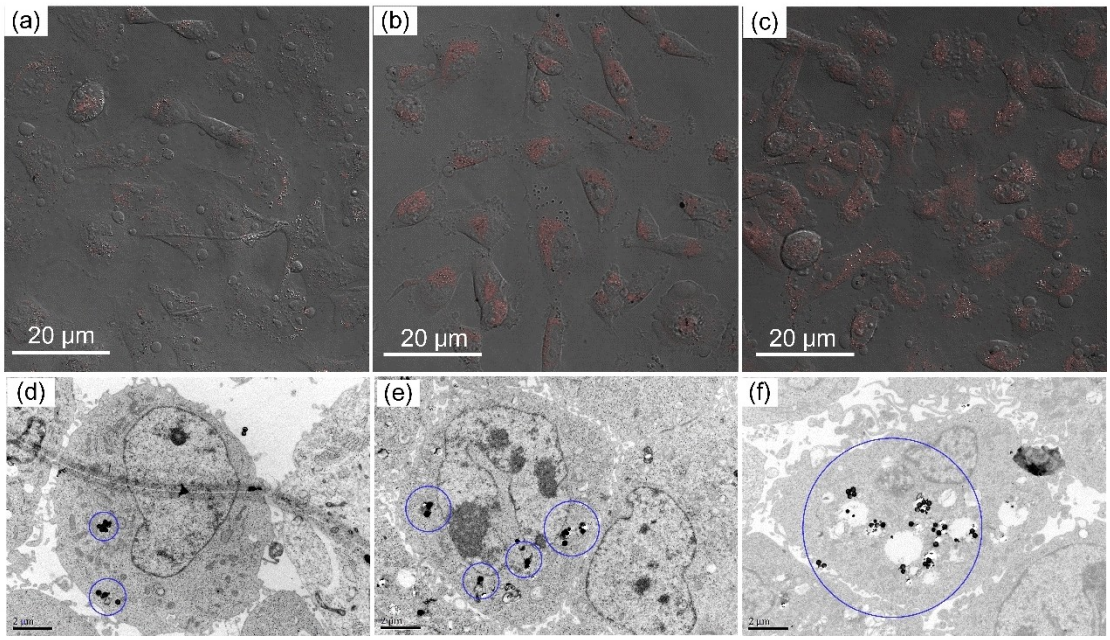

Figure 4. Confocal fluorescence images of HOS cells after incubation with a concentration of (a) 0.2 mM (b) 0.4 mM and (c) 0.6 mM SiO_2@Au@SiO_2@QDs composite particles for 24 h. TEM images of HOS cells treated with 0.4 mM SiO_2@Au@SiO_2@QDs composite particles incubation for (d) 4 h, (e) 12 h and (f) 24 h.

indicate that blank particles have good biocompatibility (see Figure 5(a)). When the cells treated with SiO_2@Au@SiO_2@QDs with a concentration of 0.6 mM, 0.3 mM and 0.15 mM, the cells viability keep at 98.5%, 96.2% and 95.0%, respectively. These results proved that this drug carrier has low cytotoxicity and good biocompatibility. For chemotherapy alone, composite particles loaded with DOX (simply labeled as SiO_2@Au@SiO_2@QDs-DOX) inhibited tumor cell proliferation in a significantly dose-dependent manner in the absence of irradiation. HOS cells treated with 0.6 mM SiO_2@Au@SiO_2@QDs-DOX lead to a cell viability of 47.6%, 0.3 mM for 90.7% and 0.15 mM for 99.6%, respectively. Under this natural release condition, the higher concentration of SiO_2@Au@SiO_2@QDs-DOX would lead to more DOX drug release which finally results in the generation of lower cell viability. To determine the effect of individual photothermal treatment on tumor cells, cells co-culture with different concentrations of SiO_2@Au@SiO_2@QDs were irradiated with an 808 nm laser at a power density of 1.5 W/cm^2 for 5 min, and the results are shown in Figure 5(a). For the cells treated with 0.6 mM SiO_2@Au@SiO_2@QDs, only 15.6% cells stayed alive, the survival rate had an increase to 87% for the case of 0.3 mM and 98.4% for the 0.15 mM case. From the above results, it can be found that, under the same irradiation conditions, a higher concentration of plasmonic particles induced more heat generation and further leaded to a higher temperature which could kill cancer cells more effectively. The cell survival rate has an evident thermal dose-dependent during the photothermal therapy process.

The inhibition efficiency of different concentrations of SiO_2@Au@SiO_2@QDs-DOX in chemotherapy-photothermal thermotherapy treatment under irradiation has also been investigated. As shown in Figure 5(a), a dose-dependent inhibition effect was exhibited in all groups. When the cells treated with 0.6 mM, 0.3 mM and 0.15 mM SiO_2@Au@SiO_2@QDs-DOX and under the irradiation, the cells viability stays at 9.1%, 55.8% and 96.3%, respectively. For the case of 0.6 mM SiO_2@Au@SiO_2@QDs-DOX, the cells had a survival rate of 9.1% which is lower than the unloaded drug case (0.6 mM SiO_2@Au@SiO_2@QDs under irradiation, the cell viability 15.6%). Although the enhanced destruction efficiency is not obvious, a synergetic therapeutic effect which combined the chemo and photothermal therapy was achieved. The possible reason for this phenomenon can be ascribed to that the photothermal therapy dominates the chemo-photothermal therapy when the concentration of plasmonic particle is very high. The real-time temperature monitoring shown in Figure 5(b) had verified this deduction. At the concentration of 0.6 mM, the plasmonic induced temperature had raised to 44.0 °C, which is located at the hyperthermia range and can killed the cells directly. The thermal-accelerated drug release would be suppressed for this case. For 0.3 mM, the combined chemotherapy-photothermal therapy was found to have a stronger inhibitory efficiency than chemotherapy or photothermal therapy alone. When the cells treated by chemo or photothermal therapy only, the cell viability stayed at 90.7% and 96.2%, however, the cell viability was 55.8% experienced a combined chemo-photothermal therapy. Scanning the temperature variation induced by plasmonic resonance heating, the temperature of the culture media reached to 37.5 °C (see Figure 5(b)) which is lower than the hyperthermia temperature, so the photothermal therapy has little effect on cell viability and only cause 3.8% on cell lethality rate. But this thermal dose was enough to accelerate

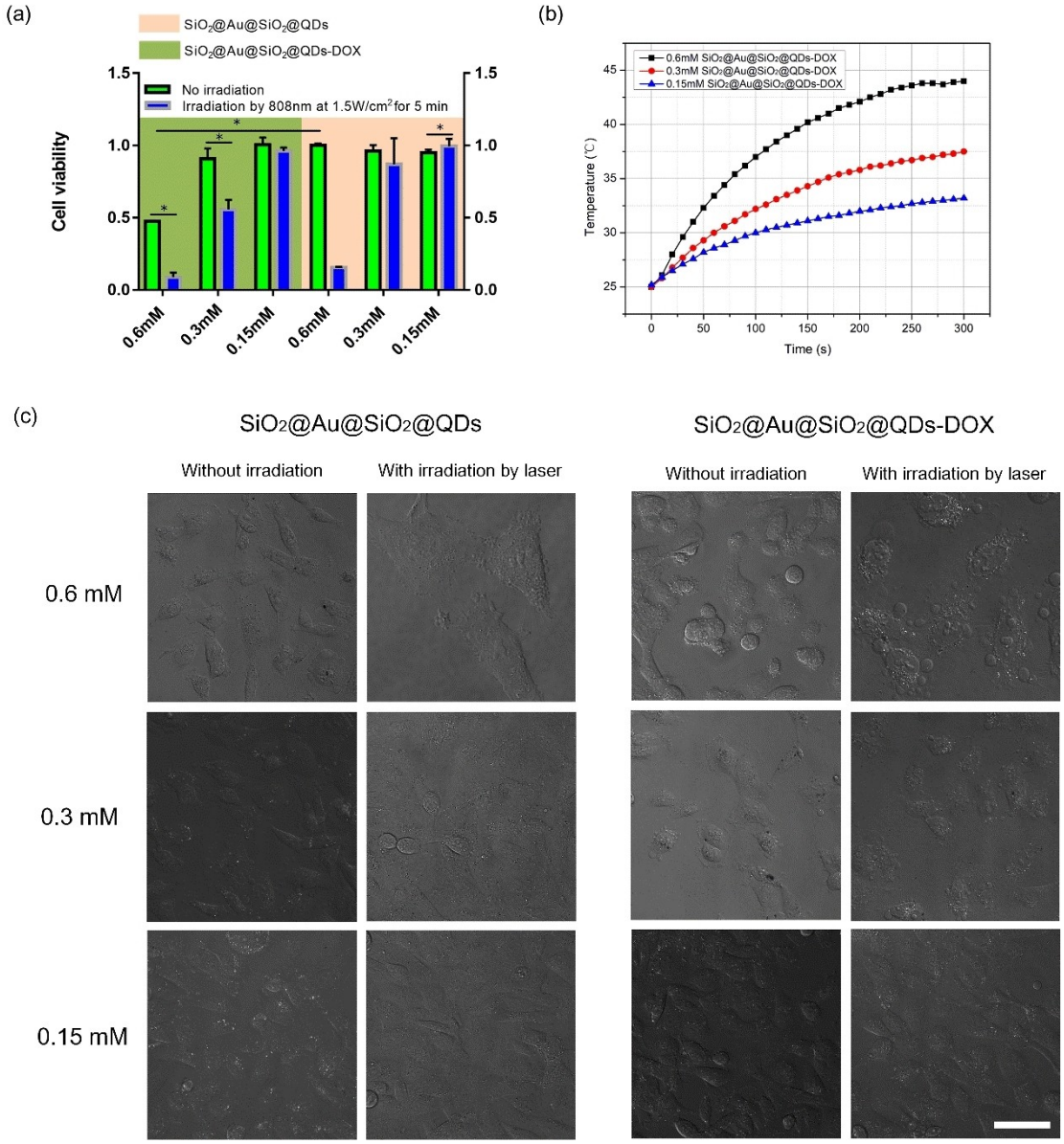

Figure 5. (a) Comparison of cell viability after DOX release in HOS cells treated with different concentrations of SiO_2@Au@SiO_2@QDs and SiO_2@Au@SiO_2@QDs-DOX particles under the 808 nm laser light or not. The data are shown as mean ± SD (n = 3). Error bars are based on three measurements. Unpaired t-tests were used. *$p < 0.05$. (b) Temperature variation of SiO_2@Au@SiO_2@QDs-DOX particle solutions with different concentrations under 808 nm laser irradiation. (c) Comparison of cellular morphology after treated with photothermal therapy, chemotherapy and chemo-photothermal combined therapy.

the DOX release from the particles to inhibit cell proliferation and leaded to a survival rate 55.8% which is lower than the cells treated with chemo or photothermal therapy only, indicating a congenerous treatment effect was reached at this concentration. For the case of 0.15 mM, the cell viability has a comparable rate with the blank group. Combined with the temperature evolution from Figure 5(b), the temperature of this case reach to 33.2 °C which is far lower than the hyperthermia temperature and also can't trigger the chemo therapy induced by heating-dependent drug accelerated release. Owing to the low concentration of SiO_2@Au@SiO_2@QDs-DOX, the loading capacity of drug is little enough to affect the cell survival rate. Cellular state diagram under different treatments is showed in Figure 5(c) which is consistent with the previous cellular viability data, further indicating this nanoplatform can combine hyperthermia and chemotherapy together and shows synergistic therapeutic effects.

Conclusions

This paper presents an experimental study on the synergistic treatment of combined thermo-chemotherapy with photothermal heating and thermal sensing of bifunctional composite particles loaded with drugs to achieve quantitative thermal dose delivery in vitro. The morphology of the composite

particles was observed by transmission electron microscopy (TEM), the elemental components were mapped by EDS attachment of TEM, and the optical properties such as UV-Vis and fluorescence emission were characterized by spectroscopy. The calibration of the bifunctional properties of the particles was achieved by irradiating the composite particle solution with near-infrared excitation light, and a linear equation for the peak wavelength fitting of the temperature-sensitive fluorescence of the composite particle solution was obtained, and a temperature-sensitivity coefficient of 0.15 nm/°C was obtained for the calibration. The cellular internalization of the composite particles was achieved by liposome transfection method, and the cellular uptake efficiency of the composite particles was found to be positively correlated with the particle concentration and incubation time by fluorescence microscopy images and transmission electron microscopy of cell sections. The photo-excitation drug release file of the drug-loaded particles was evaluated by measuring the absorption spectra of DOX molecules at 480 nm wavelength, and it was found that: the temperature of the drug-loaded particle solution gradually increased with the increase of the excitation intensity, providing more energy to open the binding energy between the drug molecules and the particles, and then more drug molecules were found to be released. By comparing the damage effects of chemotherapy alone, thermotherapy alone and the combined effect of thermo-chemotherapy on cancer cells through images of cell morphological changes and the use of cell viability tests, it was confirmed that the controlled thermal dose delivery facilitated the release of drug molecules, which in turn allowed the combination of thermo-chemotherapy to serve a synergistic therapeutic function.

Experimental section

Materials and cell lines

Sodium tellurite (Na_2TeO_3, 99%), zinc chloride ($ZnCl_2$), sodium borohydride ($NaBH_4$, 96%), sodium hydroxide (NaOH), ammonium hydroxide solution ($NH_3{\bullet}H_2O$, 25 wt%) and tri-sodium citrate dehydrate were provided by Tianjin Tianli Chemical Company Limited (Tianjin, China). 2-propanol, mercaptosuccinic acid (MSA, 99.0%), mercaptopropionic acid (MPA), ethanol and formaldehyde (37%) were brought from Shanghai Zhenxing Chemical Reagents Factory (Shanghai, China). Tetrakis(hydroxymethyl)phosphonium chloride (THPC, 80% solution in water), hydrogen tetrachloroaurate (III) trihydrate ($HAuCl_4 \cdot 3H_2O$), polyvinyl pyrrolidone (PVP, MW = 40000), 3-aminopropyltrimethoxysilane (APTMS, 97%), poly(allylamine hydrochloride) (PAH) were purchased from Sigma-Aldrich. Tetraethylorthosilicate (TEOS, 98%) was supplied by Aladdin Chemistry (Shanghai, China). HPLC grade water is used for each reaction process and for each wash process. All other reagents are of analytical grade and do not require further purification prior to use.

Cell lines. Human osteosarcoma cells (HOS cells) used in this study were supplied by the Air Force Military Medical University and maintained in RPMI 1640 supplemented with 10% fetal bovine serum and 1% penicillin-streptomycin (Hyclone). Cells were cultured in a 37 °C incubator with a humidified 5% CO2 atmosphere (Thermo Fisher Scientific Inc.).

Synthesis of SiO_2@Au@SiO_2@QDs

The synthetic method of SiO_2@Au@SiO_2@QDs particles can be followed our early publication.[14] A synthetic method route is given concisely here. The method begins with making the SiO_2@Au nanoshell using "seed and growth" approach, followed by the silica layer coating onto the golden shell with the help of modification of PVP. At the final step, the temperature sensitive QDs were anchored on the grown silica layer.

Materials and thermal characterization

Transmission electron microscope (TEM, Model: JEM–F200) was used to characterize the morphology of particles and the elemental composition distribution maps were analytically imaged by an energy dispersive X-ray spectroscopy (EDS) accessory. The fluorescence spectra were obtained by fluorescence spectrometer spectroscopy (model: Ocean Optics QE-pro). The cellular images were captured by a laser confocal scanning microscopy (Model: Nikon A1R).

An experimental system for simultaneous heating/thermometry was constructed in our laboratory, as detailed in a previous paper.[24] The system consists of complex optics, microscopes, light sources, and EMCCD cameras and spectrograph analyzers. Two light sources of different frequencies were employed, with an 808 nm near-infrared laser to activate gold nanoshells for plasmonic heating while a mercury lamp to excite the QDs for PL emission. To calibrate the thermometry, a sample SiO_2@Au@SiO_2@QDs solution was placed on a hot plate in the experimental system. The temperature variation is monitored with a thermocouple insert into the solution, and the PL emission spectra are collected and introduced into the spectrometer after the particle solution reaches a thermally stable state. The PL peak shifts were then determined as a function of temperature. After the calibration, the 808 nm laser was switched on as photothermal stimuli to induce plasmonic heating and further detect the temperature variation according to the previous established relationship between PL spectra response to the thermal variation.

Drug loading and release

SiO_2@Au@SiO_2@QDs composite particle solution (20 mL) was mixed with 10 mL doxorubicin hydrochloride (DOX) with a concentration of 1 mg/mL. The mixture was stirred for 24 hours to ensure a balanced state of drug loading. Immediately after, the pellets that had been loaded with DOX drug were centrifuged, then washed with phosphate buffer (PBS) and the supernatant was collected, and the light absorption at 480 nm was measured by UV-Vis spectrophotometer to check the loading dose of DOX. Drug retardation experiments was conducted with and without NIR laser irradiating. The samples were centrifuged at different time intervals and the supernatant was collected and analyzed by spectrograph while the precipitation was dispersed by equal volume of fresh PBS solution again for further release measurement.[26]

Cellular uptake of SiO_2@Au@SiO_2@QDs composite particles

Human osteosarcoma (HOS) cells were provided by the Air Force Medical University and cultured in RPMI 1640 supplemented with 10% fetal bovine serum and 1% penicillin (Hyclone). Liposome transfection methods have been chosen for cellular transport, where liposomes are used as carriers to transport particles across the membrane structure to the interior of the cell. A density of 1.5×10^5 HOS cell suspension of 1 mL was added to a 20 mm confocal culture dish for plate spreading and grown adductively at 37 °C

under 5% CO_2 atmosphere for 24 h (Thermo Fisher Scientific Inc.). At this point, SiO_2@Au@SiO_2@QDs composite particles dispersed in the culture medium solution were internalized into the cells using the Lipofectamine 2000 kit (Invitrogen).[24] The specific experimental procedure can be referred to our previous published paper.[14]

Acknowledgements

This work was supported by a grant from the National Natural Science Foundation of China (No.52105561), National Key R&D Program of China (2021YFB2012500), the China Postdoctoral Science Foundation (No.2020 M673379, 2020 M684466) and the University Joint Project-Key Projects of Shaanxi Province (No.2021GXLH-Z-042). The authors are grateful to the Med-X Institute of the First Affiliated Hospital of Xi'an Jiaotong University for the cellular experiments and characterization.

Conflict of Interest

The authors declare no conflict of interest.

Data Availability Statement

The data that support the findings of this study are openly available in photothermal therapy at https://doi.org/ [photo-thermal-chemotherapy], reference number 2022.

Keywords: Biological and Medicinal Chemistry · Biosensors · Cancer · Cell adhesion · Photothermal therapy

[1] a) L. C. Rogers, R. R. Davis, N. Said, T. Hollis, L. W. Daniel, *Redox Biol.* **2018**, *15*, 380–386; b) E. Pérez-Herrero, A. Fernández-Medarde, *Eur. J. Pharm. Biopharm.* **2015**, *93*, 52–79.

[2] a) Y. Wen, X. Chen, X. Zhu, Y. Gong, G. Yuan, X. Qin, J. Liu, *ACS Appl. Mater. Interfaces* **2019**, *11*, 43393–43408; b) J. Gao, F. Wang, S. Wang, L. Liu, K. Liu, Y. Ye, Z. Wang, H. Wang, B. Chen, J. Jiang, J. Ou, J. C. M. van Hest, F. Peng, Y. Tu, *Adv. Sci.* **2020**, *7*, 1903642; c) W. Ni, J. Wu, H. Fang, Y. Feng, Y. Hu, L. Lin, J. Chen, F. Chen, H. Tian, *Nano Lett.* **2021**, *21*, 7796–7805.

[3] a) D. Maiti, X. Tong, X. Mou, K. Yang, *Front. Pharmacol.* **2019**, *9*(1401); b) J. B. Vines, J.-H. Yoon, N.-E. Ryu, D.-J. Lim, H. Park, *Front. Chem.* **2019**, *7*; c) D.-P. Yang, X. Liu, C. P. Teng, C. Owh, K. Y. Win, M. Lin, X. J. Loh, Y.-L. Wu, Z. Li, E. Ye, *Nanoscale* **2017**, *9*, 15753–15759; d) E. Qiu, X. Chen, D.-P. Yang, M. D. Regulacio, R. M. C. R. Ramos, Z. Luo, Y.-L. Wu, M. Lin, Z. Li, X. J. Loh, E. Ye, *ACS Omega* **2022**, *7*, 2031–2040.

[4] a) J. Liao, W. Li, J. Peng, Q. Yang, H. Li, Y. Wei, X. Zhang, Z. Qian, *Theranostics* **2015**, *5*, 345–356; b) M. Abbasian, F. Mahmoodzadeh, R. Salehi, A. Amirshaghaghi, *New J. Chem.* **2017**, *41*, 12777–12788; c) J. Nam, S. Son, L. J. Ochyl, R. Kuai, A. Schwendeman, J. J. Moon, *Nat. Commun.* **2018**, *9*, 1074.

[5] a) E. Ye, K. Y. Win, H. R. Tan, M. Lin, C. P. Teng, A. Mlayah, M.-Y. Han, *JACS.* **2011**, *133*, 8506–8509; b) C. P. Teng, T. Zhou, E. Ye, S. Liu, L. D. Koh, M. Low, X. J. Loh, K. Y. Win, L. Zhang, M.-Y. Han, *Adv. Healthcare Mater.* **2016**, *5*, 2122–2130.

[6] a) E. C. Ximendes, U. Rocha, C. Jacinto, K. U. Kumar, D. Bravo, F. J. López, E. M. Rodríguez, J. García-Solé, D. Jaque, *Nanoscale* **2016**, *8*, 3057–3066; b) I. E. Kolesnikov, E. V. Golyeva, A. A. Kalinichev, M. A. Kurochkin, E. Lähderanta, M. D. Mikhailov, *Sens. Actuators B* **2017**, *243*, 338–345; c) C. L. West, A. C. V. Doughty, K. Liu, W. R. Chen, *J. Bio-X Res.* **2019**, *2*, 159–168.

[7] Y. A. Cheon, J. H. Bae, B. G. Chung, *Langmuir* **2016**, *32*, 2731–2736.

[8] Z. Li, E. Ye, David, R. Lakshminarayanan, X. J. Loh, *Small* **2016**, *12*, 4782–4806.

[9] S. Freddi, L. Sironi, R. D'Antuono, D. Morone, A. Donà, E. Cabrini, L. D'Alfonso, M. Collini, P. Pallavicini, G. Baldi, D. Maggioni, G. Chirico, *Nano Lett.* **2013**, *13*(5), 2004–2010.

[10] K. Nigoghossian, S. Ouellet, J. Plain, Y. Messaddeq, D. Boudreau, S. J. L. Ribeiro, *J. Mater. Chem. B* **2017**, *5*, 7109–7117.

[11] E. N. Cerón, D. H. Ortgies, B. del Rosal, F. Ren, A. Benayas, F. Vetrone, D. Ma, F. Sanz-Rodríguez, J. G. Solé, D. Jaque, E. M. Rodríguez, *Adv. Mater.* **2015**, *27*, 4781–4787.

[12] L. M. Maestro, P. Haro-González, M. C. I.-d. I. Cruz, F. SanzRodríguez, Á. Juarranz, J. G. Solé, D. Jaque, *Nanomedicine* **2013**, *8*, 379–388.

[13] B. del Rosal, E. Carrasco, F. Ren, A. Benayas, F. Vetrone, F. Sanz-Rodríguez, D. Ma, Á. Juarranz, D. Jaque, *Adv. Funct. Mater.* **2016**, *26*, 6060–6068.

[14] X. Jiang, B. Q. Li, X. Qu, H. Yang, J. Shao, H. Zhang, *Langmuir* **2019**, *35*, 6367–6378.

[15] S. L. Westcott, S. J. Oldenburg, T. R. Lee, N. J. Halas, *Langmuir* **1998**, *14*, 5396–5401.

[16] B. Sadtler, A. Wei, *Chem. Commun.* **2002**, *15*, 1604–1605.

[17] X. Jiang, W. Yu, S. Ding, B. Q. Li, *Colloids Surf. A* **2013**, *436*, 579–588.

[18] L. Deng, L. Liu, C. Zhu, D. Li, S. Dong, *Chem. Commun.* **2013**, *49*, 2503–2505.

[19] B. Xu, B. Cai, M. Liu, H. Fan, *Nanotechnology* **2013**, *24*, 205601.

[20] A. O. Yalcin, B. Goris, R. J. A. van Dijk-Moes, Z. Fan, A. K. Erdamar, F. D. Tichelaar, T. J. H. Vlugt, G. Van Tendeloo, S. Bals, D. Vanmaekelbergh, H. W. Zandbergen, M. A. van Huis, *Chem. Commun.* **2015**, *51*, 3320–3323.

[21] a) Y. Li, H. Lin, C. Luo, Y. Wang, C. Jiang, R. Qi, R. Huang, J. Travas-sejdic, H. Peng, *RSC Adv.* **2017**, *7*, 32225–32228; b) J. Liu, X. Yang, K. Wang, R. Yang, H. Ji, L. Yang, C. Wu, *Chem. Commun.* **2011**, *47*, 935–937; c) S. Patra, A. Samanta, *J. Phys. Chem. C* **2014**, *118*, 18187–18196.

[22] a) B. Ji, E. Giovanelli, B. Habert, P. Spinicelli, M. Nasilowski, X. Xu, N. Lequeux, J.-P. Hugonin, F. Marquier, J.-J. Greffet, B. Dubertret, *Nat. Nanotechnol.* **2015**, *10*, 170–175; b) N. Zhou, T. Liu, D. Li, D. Yang, *Nanomater. Nanotechnol.* **2016**, *6*, 16.

[23] W. W. Yu, L. Qu, W. Guo, X. Peng, *Chem. Mater.* **2003**, *15*, 2854–2860.

[24] X. Jiang, B. Q. Li, X. Qu, H. Yang, H. Liu, *J. Mater. Chem. B* **2017**, *5*, 8983–8990.

[25] A. Madhusudhan, G. B. Reddy, M. Venkatesham, G. Veerabhadram, D. A. Kumar, S. Natarajan, M.-Y. Yang, A. Hu, S. S. Singh, *Int. J. Mol. Sci.* **2014**, *15*, 8216–8234.

[26] Y. Huang, F. Rosei, F. Vetrone, *Nanoscale* **2015**, *7*, 5178–5185.

Manuscript received: November 30, 2022
Revised manuscript received: January 9, 2023
Accepted manuscript online: January 12, 2023
Version of record online: January 27, 2023